Electronic Supplementary Material (ESI) for Sustainable Energy & Fuels.

Supporting Information

$SnNb_2O_6$ nanosheets for electrocatalytic NRR: dual-active-center mechanism of Nb_{3c} and Sn_{4c}-Nb_{5c} dimer

Xiaotian Li [1#], Ye Tian [2#], Xiaomiao Wang [2], Yali Guo [1], Ke Chu [1*]

[1] *School of Materials Science and Engineering, Lanzhou Jiaotong University, Lanzhou 730070, China*

[2] *Department of Physics, College of Science, Hebei North University, Zhangjiakou 075000, Hebei, China*

*Corresponding author. E-mail address: chukelut@163.com (K. Chu)

[#] These authors contributed equally to this work.

Experimental Section

Synthesis of $SnNb_2O_6$

All the chemicals are of analytical grade and used as received. $SnNb_2O_6$ nanosheets were prepared by a two-step hydrothermal approach based on a reported method with a slight modification[1]. Briefly, 0.5 g of Nb_2O_5 and 2.24 g of KOH were dissolved in 30 mL of deionized water under stirring for 10 min, which were hydrothermally treated in a Teflon-lined stainless-steel autoclave for 36 h. Afterwards, 0.42 g of $SnCl_2{\cdot}2H_2O$ was added into the autoclave and the pH value was adjusted to 3 by HCl under vigorous stirring. The above mixed solution was secondly hydrothermally treated in a Teflon-lined stainless-steel autoclave for 36 h. After cooling to room temperature, the obtained $SnNb_2O_6$ were washed with deionized water and ethanol several times, and dried at 60 ^oC overnight.

Electrochemical experiments

Electrochemical measurements were carried out on a CHI-760E electrochemical workstation using a conventional three-electrode cell[2]. The catalyst coated on carbon cloth (CC) was used as the working electrode, Ag/AgCl (saturated KCl) electrode was used as the reference electrode, and graphite rod was used as the counter electrode. All potentials were referenced to reversible hydrogen electrode (RHE) on the basis of E_{RHE} (V)=$E_{Ag/AgCl}$+0.197+0.059×pH. The CC (1 × 1 cm^2) was pretreated by soaking it in 0.5 M H_2SO_4 for 12 h, and then washed with deionized water several times and dried in air. The working electrode was fabricated by coating 20 μL of the catalyst ink onto the pretreated CC (0.2 mg cm^{-2}) and dried in the air. The catalyst ink was fabricated by ultrasonically dispersing 1 mg of the catalyst in 100 μL of ethyl alcohol containing 5 μL of Nafion (5 wt%). The NRR tests were performed using an H-type two-compartment electrochemical cell separated by a Nafion 211 membrane. The Nafion membrane was pretreated by boiling it in 5% H_2O_2 solution for 1 h, 0.5 M H_2SO_4 for 1 h and deionized water for 1 h in turn. During each electrolysis, ultra-high-purity N_2 gas (99.999%) was continuously purged into the cathodic chamber at a flow rate of 20 mL min^{-1}. After each NRR electrolysis,

the produced NH_3 and possible N_2H_4 were quantitatively determined by the indophenol blue method[3], and approach of Watt and Chrisp[4], respectively. The detailed procedures for determining the concentrations of NH_3 and possible N_2H_4 have been provided in our previous works [5-7].

Characterizations

X-ray diffraction (XRD) pattern was recorded on a Rigaku D/max 2400 diffractometer. X-ray photoelectron spectroscopy (XPS) analysis was conducted on a PHI 5702 spectrometer. Transmission electron microscopy (TEM), high-angle annular dark-field scanning transmission electron microscopy (HAADF-STEM) and high-resolution transmission electron microscopy (HRTEM) were performed on a Tecnai G^2 F20 microscope. ^1H nuclear magnetic resonance (NMR) measurements were carried out on a 500 MHz Bruker superconducting-magnet NMR spectrometer. The UV-vis absorbance measurements were recorded on a MAPADA P5 spectrophotometer.

Calculation details

Spin-polarized density functional theory (DFT) calculations were conducted using a Cambridge sequential total energy package (CASTEP) [8]. The Perdew–Burke–Ernzerhof (PBE) generalized gradient approximation (GGA) functional was used for the exchange-correlation potential [8]. A cutoff energy of 650 eV is chosen and the convergence criteria of force and energy were set to be 0.01 eV $Å^{-1}$ and 1.0×10^{-5} eV, respectively. The seven-layered $SnNb_2O_6$ slab with a 2×2 supercell were constructed for slab modeling and a vacuum space of 15 Å was applied to all calculations to avoid interactions between periodic images.

The Gibbs free energy (ΔG, 298 K) of reaction steps is calculated by [9]:

$$\Delta G=\Delta E+\Delta ZPE-T\Delta S \quad (1)$$

where ΔE is the adsorption energy, ΔZPE is the zero point energy difference and $T\Delta S$ is the entropy difference between the gas phase and adsorbed state. The entropies of free gases were acquired from the NIST database.

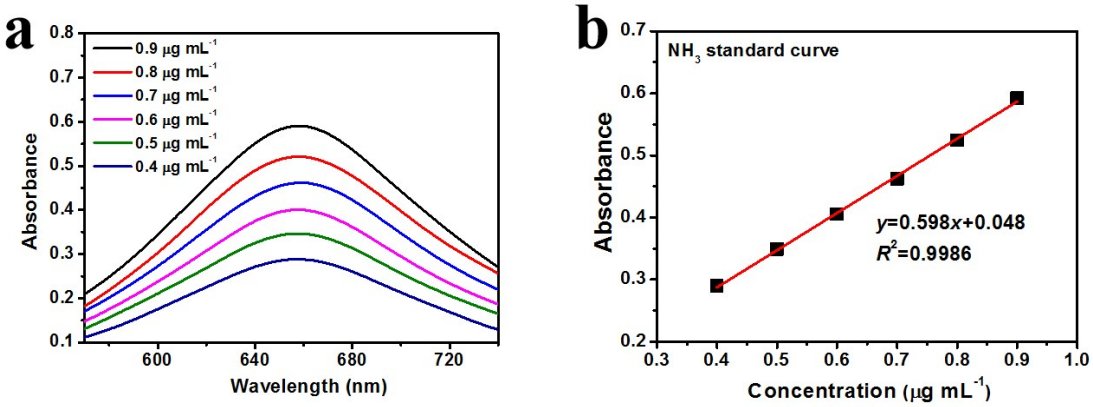

Fig. S1. (a) UV-vis absorption spectra of indophenol assays with NH_4Cl after incubated for 2 h at ambient conditions. (b) Calibration curve used for calculation of NH_3 concentrations.

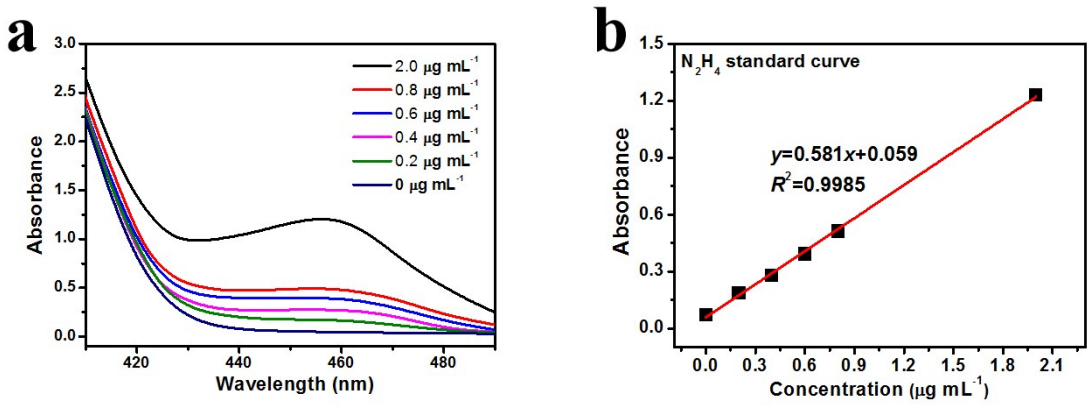

Fig. S2. (a) UV-vis absorption spectra of N_2H_4 assays after incubated for 20 min at ambient conditions. (b) Calibration curve used for calculation of N_2H_4 concentrations.

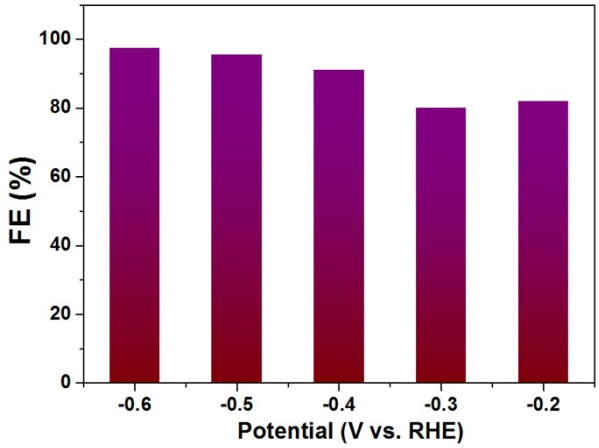

Fig. S3. FE of H_2 production at various potentials over $SnNb_2O_6$.

The FE for H_2 yield can be calculated by [10]

$$\text{FE}\ (\%) = \frac{2 \times F \times n}{Q} \times 100\% \qquad (2)$$

where Q is the quantity of applied electricity. F is the Faraday constant, n is the actually produced H_2 (mol) obtained by gas chromatography (GC-2014C, Shimadzu) which is directly connected to the cathodic compartment[11]. Based on the FE data for H_2 production with the FE for NH_3 selectivity (Fig. 2d), the unaccounted values is possibly derived from the dynamic hydrogen adsorption on the catalyst, the capacitance of the support and the uncontrollable experimental error[12].

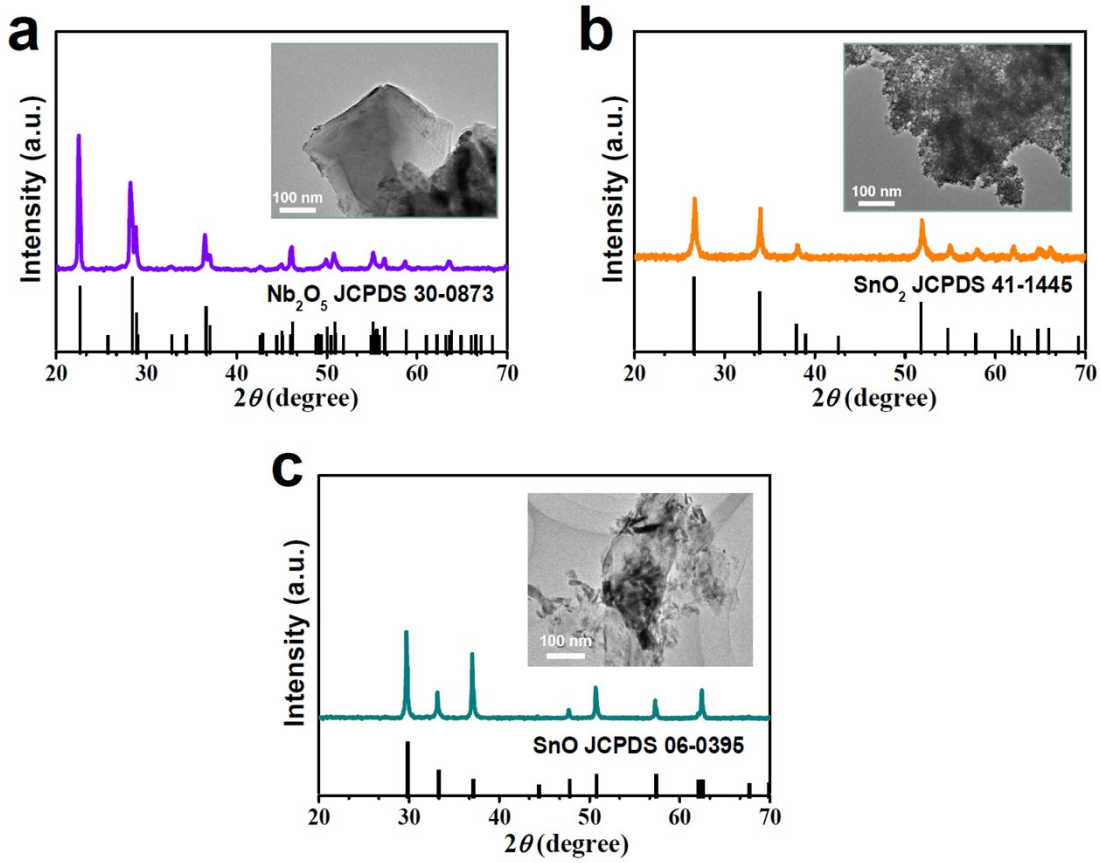

Fig. S4. (a) XRD pattern of Nb_2O_5 nanosheets (inset: TEM image). (b) XRD pattern of SnO_2 nanosheets (inset: TEM image). (c) XRD pattern of SnO nanosheets (inset: TEM image). The Nb_2O_5 nanosheets, SnO_2 nanosheets and SnO nanosheets were prepared based on the reported methods of [13], [14] and [15], respectively.

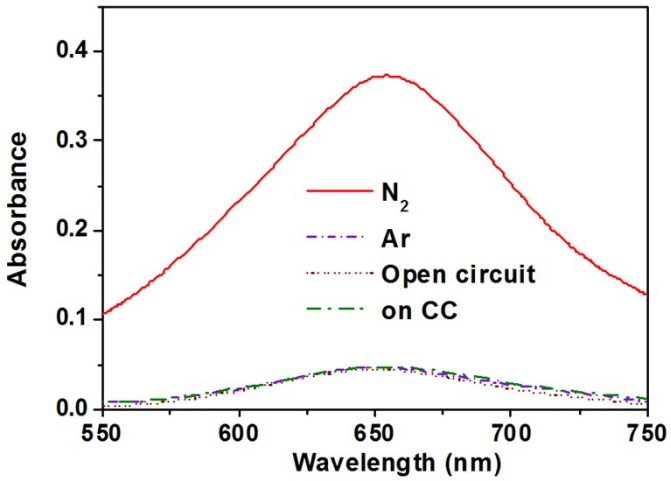

Fig. S5. UV-vis absorption spectra of working electrolytes after 2 h of electrolysis on $SnNb_2O_6$ at -0.3 V (vs. RHE) in N_2-saturated solution, Ar-saturated solutions, N_2-saturated solution at open circuit and N_2-saturated solution on pristine CC.

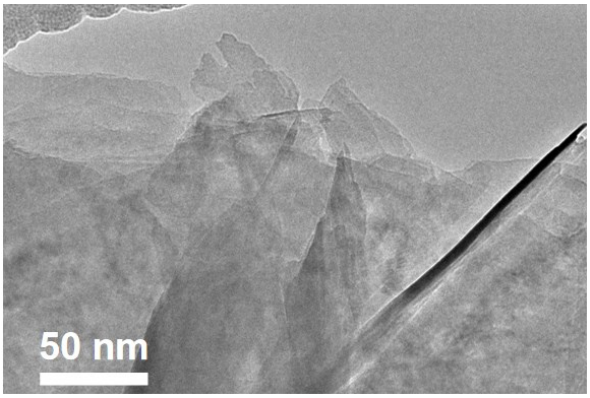

Fig. S6. TEM image of $SnNb_2O_6$ after stability test.

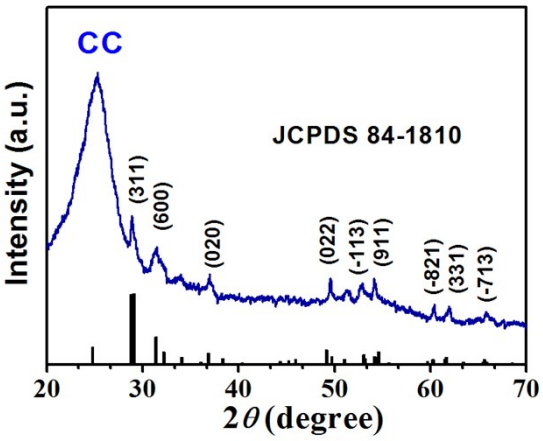

Fig. S7. XRD pattern of $SnNb_2O_6$ after stability test.

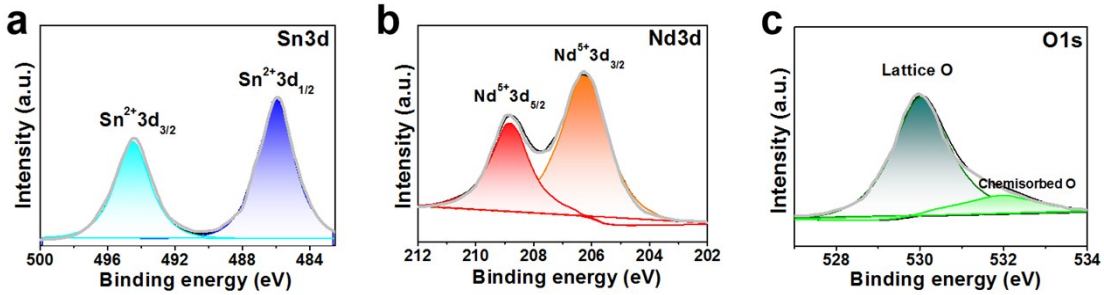

Fig. S8. XPS spectra of $SnNb_2O_6$ nanosheets after stability test: (a) Sn3d; (b) Nd3d; (c) O1s.

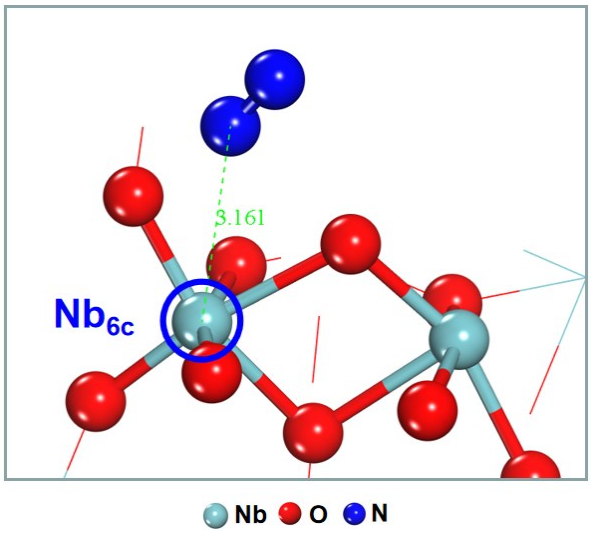

Fig. S9. Optimized structure of N_2 adsorption on Nb_{6c} site of $SnNb_2O_6$ (311) .

Table S1. Comparison of optimum NH_3 yield and Faradic efficiency (FE) for recently reported state-of-the-art NRR electrocatalysts at ambient conditions

Catalyst	Electrolyte	Determination method	Optimum Potential (V Vs RHE)	NH_3 yield ($\mu g\ h^{-1}\ mg^{-1}$)	FE (%)	Ref.
Pd/C	0.1 M PBS	Indophenol blue method	0.1	4.5	8.2	[16]
Mo single atoms	0.1 M KOH	Indophenol blue method	-0.3	34	14.6	[17]
Ru single atoms/NPC	0.05 M H_2SO_4	Indophenol blue method	-0.2	120.9	29.6	[18]
MoO_3 nanosheets	0.1 M HCl	Indophenol blue method	-0.5	29.43	1.9	[19]
Mo_2C/C	0.5 M Li_2SO_4	Nessler's reagent method	-0.3	11.3	7.8	[20]
$BiVO_4$ with oxygen vacancies	0.2 M Na_2SO_4	Indophenol blue method	-0.5	8.6	10.4	[21]
MoS_2 with Li-S Interactions	0.1 M Li_2SO_4	Indophenol blue method	-0.2	43.4	9.81	[22]
S-doped carbon nanospheres	0.1 M Na_2SO_4	Indophenol blue method	-0.7	19.07	7.47	[23]
Cubic sub-micron SnO_2 particles	0.1 M Na_2SO_4	Indophenol blue method	-0.7	4.03	2.17	[24]
F-doped SnO_2	0.1 M Na_2SO_4	Indophenol blue method	-0.45	19. 3	8.6	[25]
Fe-doped SnO_2	0.1 M HCl	Indophenol blue method	-0.3	82.7	20.4	[26]
SnO_2/RGO	0.1 M Na_2SO_4	Indophenol blue method	-0.5	25.6	7.1	[27]
Nb_2O_5 nanofibers	0.1 M HCl	Indophenol blue method	-0.55	43.6	9.26	[12]
NbO_2 nanoparticles	0.05 M H_2SO_4	Indophenol blue method	-0.65	11.6	32 (-0.6)	[28]
$SnNb_2O_6$	**0.5 M $LiClO_4$**	**Indophenol blue method**	**-0.3**	**53.1**	**17.6**	**This work**

Supplementary references

[1]. Z. Zhang, D. Jiang, D. Li, M. He and M. Chen, *Appl. Catal. B*, 2016, **183**, 113-123.

[2]. Q. Li, Y. Cheng, X. Li, Y. Guo and K. Chu, *Chem. Commun.*, 2020, **56**, 13009-13012.

[3]. D. Zhu, L. Zhang, R. E. Ruther and R. J. Hamers, *Nat. Mater.*, 2013, **12**, 836.

[4]. G. W. Watt and J. D. Chrisp, *Anal. Chem.*, 1952, **24**, 2006-2008.

[5]. W. Gu, Y. Guo, Q. Li, Y. Tian and K. Chu, *ACS Appl. Mater. Inter.*, 2020, **12**, 37258-

37264.
[6]. K. Chu, J. Wang, Y. P. Liu, Q. Q. Li and Y. L. Guo, *J. Mater. Chem. A*, 2020, **8**, 7117-7124.
[7]. K. Chu, Y. P. Liu, Y. B. Li, Y. L. Guo and Y. Tian, *ACS Appl. Mater. Inter.*, 2020, **12**, 7081-7090.
[8]. S. J. Clark, M. D. Segall, C. J. Pickard, P. J. Hasnip, M. I. J. Probert, K. Refson and M. C. Payne, *Z. Kristallogr.*, 2005, **220**, 567-570.
[9]. A. A. Peterson, *Energy Environ. Sci.*, 2010, **3**, 1311-1315.
[10]. X. Li, T. Li, Y. Ma, Q. Wei, W. Qiu, H. Guo, X. Shi, P. Zhang, A. M. Asiri and L. Chen, *Adv. Energy. Mater.*, 2018, **8**, 1801357.
[11]. J. Q. Tian, Q. Liu, A. M. Asiri and X. P. Sun, *J. Am. Chem. Soc.*, 2014, **136**, 7587-7590.
[12]. J. Han, Z. Liu, Y. Ma, G. Cui, F. Xie, F. Wang, Y. Wu, S. Gao, Y. Xu and X. Sun, *Nano Energy*, 2018, **52**, 264-270.
[13]. H. Luo, M. Wei and K. Wei, *Mater. Chem. Phys.*, 2010, **120**, 6-9.
[14]. F. Li, L. Chen, G. P. Knowles, D. R. MacFarlane and J. Zhang, *Angew. Chem. Int. Edit.*, 2017, **56**, 505-509.
[15]. H. Zhang, Q. He, F. Wei, Y. Tan, Y. Jiang, G. Zheng, G. Ding and Z. Jiao, *Mater. Lett.*, 2014, **120**, 200-203.
[16]. J. Wang, L. Yu, L. Hu, G. Chen, H. Xin and X. Feng, *Nat. Commun.*, 2018, **9**, 1795.
[17]. L. Han, X. Liu, J. Chen, R. Lin, H. Liu, F. Lu, S. Bak, Z. Liang, S. Zhao and E. Stavitski, *Angew. Chem. Int. Edit.*, 2018, **58**, 2321-2325.
[18]. Z. Geng, Y. Liu, X. Kong, P. Li, K. Li, Z. Liu, J. Du, M. Shu, R. Si and J. Zeng, *Adv. Mater.*, 2018, **30**, 1803498.
[19]. J. Han, X. Ji, X. Ren, G. Cui, L. Li, F. Xie, H. Wang, B. Li and X. Sun, *J. Mater. Chem. A*, 2018, **6**, 12974-12977.
[20]. H. Cheng, L. X. Ding, G. F. Chen, L. Zhang, J. Xue and H. Wang, *Adv. Mater.*, 2018, **30**, 1803694.
[21]. J. X. Yao, D. Bao, Q. Zhang, M. M. Shi, Y. Wang, R. Gao, J. M. Yan and Q. Jiang, *Small Methods*, 2018, **3**, 1800333.
[22]. Y. Liu, M. Han, Q. Xiong, S. Zhang, C. Zhao, W. Gong, G. Wang, H. Zhang and H. Zhao, *Adv. Energy. Mater.*, 2019, **9**, 1803935.
[23]. L. Xia, X. Wu, Y. Wang, Z. Niu, Q. Liu, T. Li, X. Shi, A. M. Asiri and X. Sun, *Small Methods*, 2018, **3**, 1800251.
[24]. L. Zhang, X. Ren, Y. Luo, X. Shi, A. M. Asiri, T. S. Li and X.-P. Sun, *Chem. Commun.*, 2018.
[25]. Y. P. Liu, Y. B. Li, H. Zhang and K. Chu, *Inorg. Chem.*, 2019, **58**, 10424-10431.
[26]. L. Zhang, M. Cong, X. Ding, Y. Jin, F. Xu, Y. Wang, L. Chen and L. Zhang, *Angew. Chem. Int. Edit.*, 2020, **132**, 10980-10985.
[27]. K. Chu, Y. Liu, Y. Li, J. Wang and H. Zhang, *ACS Appl. Mater. Inter.*, 2019, **11**, 31806-31815.
[28]. L. Huang, J. Wu, P. Han, A. M. Al-Enizi, T. M. Almutairi, L. Zhang and G. Zheng, *Small Methods*, 2019, **3**, 1800386.